



Molecular underpinnings and biogeochemical consequences of enhanced diatom growth in a warming Southern Ocean

Loay J. Jabre^a, Andrew E. Allen^{b,c,1}, J. Scott P. McCain^a, John P. McCrow^b, Nancy Tenenbaum^d, Jenna L. Spackeen^e, Rachel E. Sipler^{e,f,g}, Beverley R. Green^h, Deborah A. Bronk^{e,g}, David A. Hutchins^{d,1}, and Erin M. Bertrand^{a,1}

^aDepartment of Biology, Life Sciences Center, Dalhousie University, Halifax, NS B3H 4R2, Canada; ^bMicrobial and Environmental Genomics, J. Craig Venter Institute, La Jolla, CA 92037; ^cIntegrative Oceanography Division, Scripps Institution of Oceanography, University of California San Diego, La Jolla, CA 92037; ^dMarine and Environmental Biology, University of Southern California, Los Angeles, CA 90089; ^eVirginia Institute of Marine Science, College of William & Mary, Gloucester Point, VA 23062; ^fOcean Sciences Centre, Memorial University of Newfoundland, St. John's, NL A1C 5S7, Canada; ^gBigelow Laboratory for Ocean Sciences, East Boothbay, ME 04544; and ^hDepartment of Botany, University of British Columbia, Vancouver, BC V6T 1Z4, Canada

Edited by David M. Karl, University of Hawaii at Manoa, Honolulu, HI, and approved June 18, 2021 (received for review April 20, 2021)

The Southern Ocean (SO) harbors some of the most intense phytoplankton blooms on Earth. Changes in temperature and iron availability are expected to alter the intensity of SO phytoplankton blooms, but little is known about how these changes will influence community composition and downstream biogeochemical processes. We performed light-saturated experimental manipulations on surface ocean microbial communities from McMurdo Sound in the Ross Sea to examine the effects of increased iron availability (+2 nM) and warming (+3 and +6 °C) on nutrient uptake, as well as the growth and transcriptional responses of two dominant diatoms, *Fragilariopsis* and *Pseudo-nitzschia*. We found that community nutrient uptake and primary productivity were elevated under both warming conditions without iron addition (relative to ambient -0.5 °C). This effect was greater than additive under concurrent iron addition and warming. *Pseudo-nitzschia* became more abundant under warming without added iron (especially at 6 °C), while *Fragilariopsis* only became more abundant under warming in the iron-added treatments. We attribute the apparent advantage *Pseudo-nitzschia* shows under warming to up-regulation of iron-conserving photosynthetic processes, utilization of iron-economic nitrogen assimilation mechanisms, and increased iron uptake and storage. These data identify important molecular and physiological differences between dominant diatom groups and add to the growing body of evidence for *Pseudo-nitzschia*'s increasingly important role in warming SO ecosystems. This study also suggests that temperature-driven shifts in SO phytoplankton assemblages may increase utilization of the vast pool of excess nutrients in iron-limited SO surface waters and thereby influence global nutrient distribution and carbon cycling.

Southern Ocean | metatranscriptomics | iron limitation | temperature | diatoms

The Southern Ocean (SO) occupies less than 10% of Earth's ocean surface area but plays a major role in driving global climate and biogeochemical cycles. It connects the Pacific, Atlantic, and Indian ocean basins, supplies nutrients to lower latitudes, and absorbs a considerable portion of global heat and CO₂ (1, 2). SO ecological processes are driven by seasonally productive phytoplankton assemblages that require sufficient light, macronutrients (e.g., nitrogen, phosphorus), micronutrients (e.g., iron, vitamin B₁₂), and suitable temperatures to grow. These phytoplankton sequester atmospheric CO₂ through the biological pump, sustain food webs, and influence the stoichiometry of nutrient supply to lower latitudes. Despite large regional variations, climate change models project overall warming in the SO, with current average sea surface temperatures (0 to 4 °C) predicted to increase by 1 to 2 °C in 2100 and ~6 °C by 2300 (2–5). Additionally, small increases in iron supply (e.g., increased iron flux, by ~0.01 nM and ~0.02 nM day⁻¹ by 2100 and 2300, respectively) are projected for

the SO (2, 4) (*SI Appendix, Table S1*), but large uncertainties remain in model projections of SO iron supply, which are complicated by the diversity of supply mechanisms and other physical/chemical factors (6, 7). Temperature and iron can be major drivers of SO phytoplankton growth (8, 9), yet we still have a limited understanding of how changes in these factors will influence the cellular mechanisms that govern phytoplankton dynamics and biogeochemistry in the SO.

Low iron availability limits phytoplankton growth and is the primary cause of the high-(macro)nutrient low-chlorophyll (HNLC) conditions in the SO (9, 10). Despite this, diatoms are highly successful in these environments and contribute substantially to primary productivity throughout the region. Low-iron-adapted diatoms utilize several strategies to survive chronic, episodic, or seasonal iron limitation. For example, they can reduce photosynthetic iron demand by substituting iron-containing ferredoxin with flavodoxin (11) or cytochrome *c*₆ with plastocyanin (12). Increased light harvesting cross-section has also been observed in several iron-stressed diatoms, allowing for more light energy capture to

Significance

Phytoplankton contribute to the Southern Ocean's (SO) ability to absorb atmospheric CO₂ and shape the stoichiometry of northward macronutrient delivery. Climate change is altering the SO environment, yet we know little about how resident phytoplankton will react to these changes. Here, we studied a natural SO community and compared responses of two prevalent, bloom-forming diatom groups to changes in temperature and iron that are projected to occur by 2100 to 2300. We found that one group, *Pseudo-nitzschia*, grows better under warmer low-iron conditions by managing cellular iron demand and efficiently increasing photosynthetic capacity. This ability to grow and draw down nutrients in the face of warming, regardless of iron availability, has major implications for ocean ecosystems and global nutrient cycles.

Author contributions: A.E.A., D.A.H., and E.M.B. designed research; A.E.A., N.T., J.L.S., R.E.S., D.A.B., D.A.H., and E.M.B. performed research; A.E.A. contributed new reagents/analytic tools; L.J.J., A.E.A., J.S.P.M., J.P.M., J.L.S., R.E.S., B.R.G., D.A.B., D.A.H., and E.M.B. analyzed data; and L.J.J., A.E.A., J.S.P.M., J.L.S., R.E.S., B.R.G., D.A.B., D.A.H., and E.M.B. wrote the paper.

The authors declare no competing interest.

This article is a PNAS Direct Submission.

This open access article is distributed under [Creative Commons Attribution-NonCommercial-NoDerivatives License 4.0 \(CC BY-NC-ND\)](https://creativecommons.org/licenses/by-nc-nd/4.0/).

¹To whom correspondence may be addressed. Email: erin.bertrand@dal.ca, dahutch@usc.edu, or aallen@jvci.org.

This article contains supporting information online at <https://www.pnas.org/lookup/suppl/doi:10.1073/pnas.2107238118/-DCSupplemental>.

Published July 23, 2021.

facilitate photosynthesis (13, 14). Diatoms may also use iron-free rhodopsin to supplement photosynthetic energy capture (15), have transport mechanisms that can be up-regulated to maximize iron acquisition (16–18), and some species contain iron storage proteins (ferritin) to buffer the sporadic availability of this micronutrient (19).

Temperature influences intracellular transport processes and enzymatic turnover rates and ultimately plays an important role in controlling phytoplankton growth and physiology (20). Temperature has also been shown to limit SO phytoplankton growth in the field and the laboratory. Warming incubations that simulate projected sea surface temperature changes by the year 2100 to 2300 (0 °C versus +4 °C) in iron-limited, diatom-dominated SO microbial communities resulted in increased nutrient draw-down and improved the growth of several diatom groups (21), with similar results reported in iron-limited laboratory diatom cultures grown under the same temperature treatments (22). Warming (up to a critical threshold) improves iron use efficiency (23–25), increases the turnover rate of iron-containing enzymes such as nitrate reductase (26, 27), and may thus cause increased utilization of SO nitrate even in the absence of iron addition (7, 28). Some Antarctic diatoms such as *Fragilariopsis cylindrus* also exhibit reduced cell size under elevated temperature, which can decrease cellular iron quotas, increase surface area to volume ratios,

and facilitate nutrient uptake and growth (14). Other studies have shown a reduction in the upper thermal limit of Antarctic diatom growth (e.g., centric diatoms *Chaetoceros neglectus*, *Chaetoceros flexuosus*, *Thalassiosira antarctica*) under reduced iron availability (29, 30), and some diatoms like the pennate *F. cylindrus* still require iron supplementation (≥ 10 nM EDTA-buffered iron) to benefit from warming (3 °C and 6 °C compared to 1 °C), even when iron-conserving mechanisms are used (14). Additionally, concurrent increases in temperature and iron have been shown to have larger synergistic effects on growth and nutrient utilization compared to the individual effects of each factor (7, 21, 22). Here, we define “synergistic” as a nonlinear, multiplicative response, which exceeds the sum of the individual effects of iron and temperature (31).

Despite shared adaptations across various taxa, diatoms are an extremely diverse group of phytoplankton. Within the SO, major diatom groups have different morphological and physiological traits, with unique optimal growth temperatures and different tolerances to low iron (13, 29, 32–35). The molecular mechanisms that underpin these differences are still poorly understood and are overlooked by the majority of current marine ecosystem models, which consider all diatoms as one group (36). This oversimplification cannot capture how environmentally mediated changes in diatom community composition and structure (e.g., communities

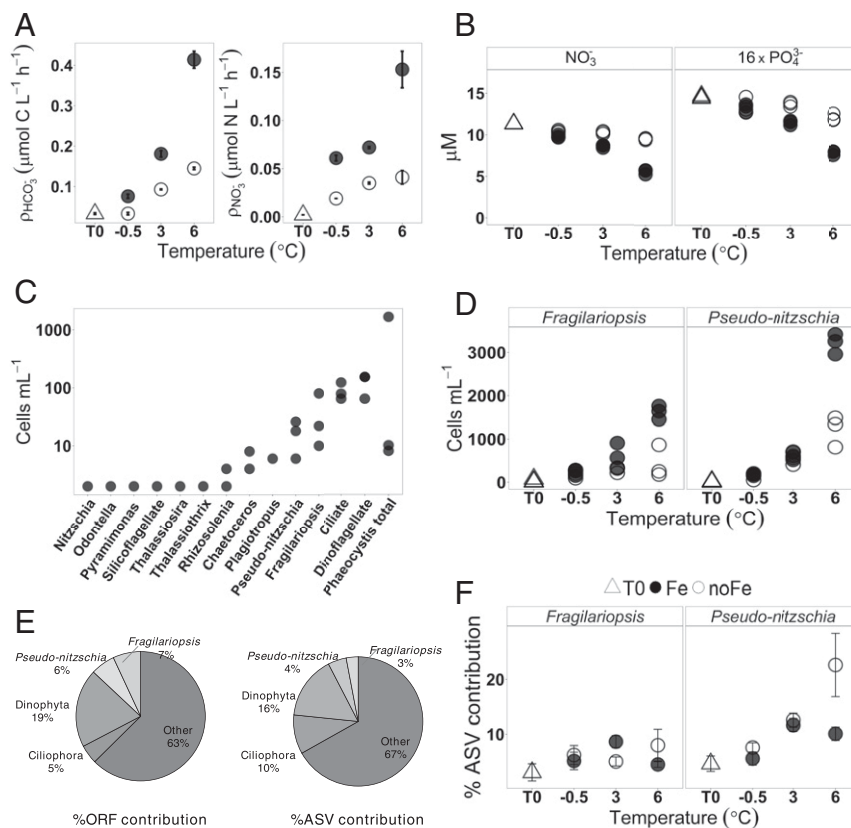


Fig. 1. (A) Absolute bicarbonate and nitrate uptake rates at T0 (prior to the incubations) and T7 for each temperature and iron condition. Uptake rates were measured in duplicate from a single incubation bottle per treatment. (B) Dissolved nitrate and phosphate concentrations in triplicate incubation bottles at T0 and T7. Phosphate concentration is scaled (16 \times) for better visual comparison with nitrate. (C) Initial (T0) cell counts of eukaryotic taxa identified by light microscopy, $n = 3$, taxa are arranged from low to high abundance. The large variation in *Phaeocystis* cell counts at T0 likely resulted from random variability in colony abundance and size in the relatively small-volume samples used for microscopic cell counts. Cell counts for other taxonomic groups under the different temperature and iron treatments are shown in *SI Appendix, Fig. S2*. (D) Measurements of *Fragilariopsis* and *Pseudo-nitzschia* cell counts at T0 and T7 in triplicate incubation bottles for each temperature and iron condition. (E) Pie charts representing percent contribution of taxa to the total reads mapped to ORFs and to the total 18S rRNA Amplicon Sequence Variant (ASV) abundance at T0. “Other” represents all other taxonomic groups, including prokaryotes and viruses. (F) Percent contribution of *Fragilariopsis* and *Pseudo-nitzschia* to the total ASV abundance at T0 and T5 for each temperature and iron condition. Each point represents triplicate means; error bars represent ± 1 SD and fall within the bounds of the symbol when not visible.

with different sinking rates) may affect important ecological processes, as well as nutrient and carbon biogeochemistry (37).

Here, we present an experimental manipulation study performed at the sea ice edge (IE) in the Ross Sea of the SO. Coastal areas of the SO, including the sea IE, are highly productive, and the Ross Sea alone contributes to ~25% of all SO primary productivity (38), making this area of the SO ecologically and biogeochemically important. This region has also been shown in previous growing seasons [e.g., 2013, 2014 (39)] to be iron limited, suggesting that despite its coastal nature, phytoplankton here experience similar nutritional stressors found throughout the Ross Sea and broader SO. We investigated the growth, nutrient drawdown, and transcriptional responses of an SO microbial community to warming and changes in iron availability, mimicking changes that are projected to occur between the years 2100 and 2300 (2–5). We show that nutrient drawdown increases in response to temperature and iron, both independently and synergistically, and that two closely related diatom groups, *Fragilariopsis* spp. and *Pseudo-nitzschia* spp., respond differently to changes in temperature and iron. These two bloom-forming taxa (40) contribute substantially to diatom assemblages in the SO and strongly influence the ecology and biogeochemistry of the region (21, 41, 42). *Pseudo-nitzschia* cell numbers increased more than *Fragilariopsis* under warming alone, while the latter required iron addition to benefit from increased temperature. Our metatranscriptome data suggest that the growth of *Pseudo-nitzschia* under warming is likely facilitated by temperature-responsive light harvesting and iron management strategies that were not utilized by *Fragilariopsis*. This ability to grow and draw down nutrients in the face of warming, regardless of iron availability, could have major implications for the ecological and biogeochemical response of the HNLC SO to a changing climate.

Results and Discussion

We incubated SO surface water under constant growth-saturating light (65 to $85 \mu\text{E m}^{-2} \text{sec}^{-1}$) with and without 2 nM iron addition at three temperatures ($-0.5 \text{ }^\circ\text{C}$, $3 \text{ }^\circ\text{C}$, $6 \text{ }^\circ\text{C}$) to simulate increased iron availability and a range of SO surface water temperatures, spanning from current to projected conditions 100 to 300 y from now (2–4) (*SI Appendix, Table S1*). We then examined the microbial community after 24 h (T1) and again after 5 (T5) and 7 d (T7). Unless otherwise stated, a temperature effect (i.e., effect of increased temperature) on the various measured parameters refers to an effect at both $3 \text{ }^\circ\text{C}$ and $6 \text{ }^\circ\text{C}$ (see *Materials and Methods Summary* for details).

Increasing temperature and iron separately caused a significant but small increase in community ($>0.7 \mu\text{m}$) primary productivity measured as bicarbonate uptake (Fig. 1A and *SI Appendix, Fig. S1*, two-way ANOVA, temperature effect $P = 1.1 \times 10^{-6}$, Fe effect $P = 2.4 \times 10^{-6}$), as well as an increase in community nitrate uptake rates (Fig. 1A and *SI Appendix, Fig. S1*, two-way ANOVA, temperature effect $P = 0.001$, Fe effect $P = 7.9 \times 10^{-5}$), nitrate consumption (Fig. 1B and *SI Appendix, Fig. S1*, two-way ANOVA, temperature effect $P = 2.9 \times 10^{-11}$, Fe effect $P = 1.2 \times 10^{-11}$), and phosphorus consumption (Fig. 1B and *SI Appendix, Fig. S1*, two-way ANOVA, temperature effect $P = 2.3 \times 10^{-6}$, Fe effect $P = 1.0 \times 10^{-6}$). Incubations under concurrent warming and iron addition showed a synergistic increase in primary productivity (Fig. 1A, two-way ANOVA, temperature \times Fe effect $P = 4.7 \times 10^{-5}$), nitrate uptake rates (Fig. 1A, two-way ANOVA, temperature \times Fe effect $P = 0.007$), nitrate consumption (Fig. 1B and *SI Appendix, Fig. S1*, two-way ANOVA, temperature \times Fe effect $P = 6.0 \times 10^{-9}$), and phosphorus consumption (Fig. 1B and *SI Appendix, Fig. S1*, two-way ANOVA, temperature \times Fe effect $P = 7.5 \times 10^{-5}$). This synergistic iron–temperature effect has been observed previously (21, 28) and suggests that future warming conditions can strongly influence SO

productivity and nutrient drawdown, especially if combined with a concurrent increase in iron availability.

Microscopy observations showed that *Phaeocystis*, dinoflagellates, ciliates, *Fragilariopsis*, and *Pseudo-nitzschia* were among the most abundant eukaryotic taxa at the beginning of the incubation experiment (the in situ community) and after temperature and iron incubations (Fig. 1C and *SI Appendix, Fig. S2*). We focused our analyses here on the responses of the two most abundant diatom groups in our samples, *Fragilariopsis* (identified by light microscopy and 18S ribosomal RNA sequencing as mostly *Fragilariopsis kerguelensis* and *Fragilariopsis cylindrus*) and *Pseudo-nitzschia* (identified by light microscopy, 18S ribosomal RNA sequencing, and a protein Basic Local Alignment Search Tool (BLAST-p) analysis of *Pseudo-nitzschia* transcriptomes as mostly *Pseudo-nitzschia subcurvata*) (reference *SI Appendix, Tables S2 and S3 and Full Materials and Methods*). *Pseudo-nitzschia* but not *Fragilariopsis* cell counts increased significantly under warming without added iron (Fig. 1D, two-way ANOVA, temperature effect $P = 0.003$ and $P = 0.5$, respectively) and showed the largest increase in abundance throughout the incubations, compared to other plankton groups (*SI Appendix, Fig. S2*). Additionally, concurrent warming and iron supplementation caused an increase in *Fragilariopsis* (Fig. 1D, two-way ANOVA, temperature \times Fe effect $P = 0.001$) and a much larger synergistic increase in *Pseudo-nitzschia* cell counts (Fig. 1D, two-way ANOVA, temperature \times Fe effect $P = 1.13 \times 10^{-6}$). This highlights the ability of *Pseudo-nitzschia* to increase its growth under warmer conditions, regardless of iron availability.

We used metatranscriptomics to comprehensively capture gene expression patterns and examine the molecular processes underpinning the distinct growth responses of *Fragilariopsis* and *Pseudo-nitzschia* to shifts in iron availability and temperature (Fig. 2). Metatranscriptomics allows for the interrogation of cellular pathways utilized across various taxa and can be used to infer metabolic states under different environmental conditions (39, 43, 44). Here, we identified transcripts belonging to viruses, prokaryotes, and eukaryotes (*SI Appendix, Fig. S3*); with dinoflagellates, ciliates, *Pseudo-nitzschia*, and *Fragilariopsis* contributing 37% of the total reads mapped to open reading frames (ORFs) (Fig. 1E). The contribution of *Phaeocystis* to the metatranscriptome was lower than anticipated based on microscopy, possibly due to difficulty in harvesting cells/colonies without rupturing them (45). Kyoto Encyclopedia of Genes and Genomes (KEGG) Orthology (KO) term enrichment analysis on ORFs belonging to *Fragilariopsis* and *Pseudo-nitzschia* showed that pathways corresponding to photosynthesis, nitrogen metabolism, and genetic information processing/translation were highly differentially expressed in both taxa following temperature and iron increase (*SI Appendix, Figs. S4 and S5*). We explored these pathways in more detail by grouping individual ORFs into clusters of similar sequences using Markov clustering (MCL) (46) (*Materials and Methods Summary*). Several clusters contained differential expression patterns that were similar in *Fragilariopsis* and *Pseudo-nitzschia* under iron addition (63 clusters) and temperature increase (212 clusters). However, a larger number of clusters were uniquely differentially expressed in either *Fragilariopsis* or *Pseudo-nitzschia* under these conditions (Fig. 3A), suggesting that *Fragilariopsis* and *Pseudo-nitzschia* utilize different molecular strategies to respond to changes in temperature and/or iron.

Photosynthesis. Iron addition resulted in up-regulation of iron-containing cytochrome b_6/f complex transcripts and down-regulation of flavodoxin transcripts in both *Fragilariopsis* and *Pseudo-nitzschia* (Figs. 2 and 3). This indicates that both diatoms in our study were undergoing some degree of iron stress at the time of sampling; ambient dissolved iron concentrations at the time of sampling were growth limiting at 0.47 nM (47), and iron-containing photosynthetic processes including the electron transport chain can

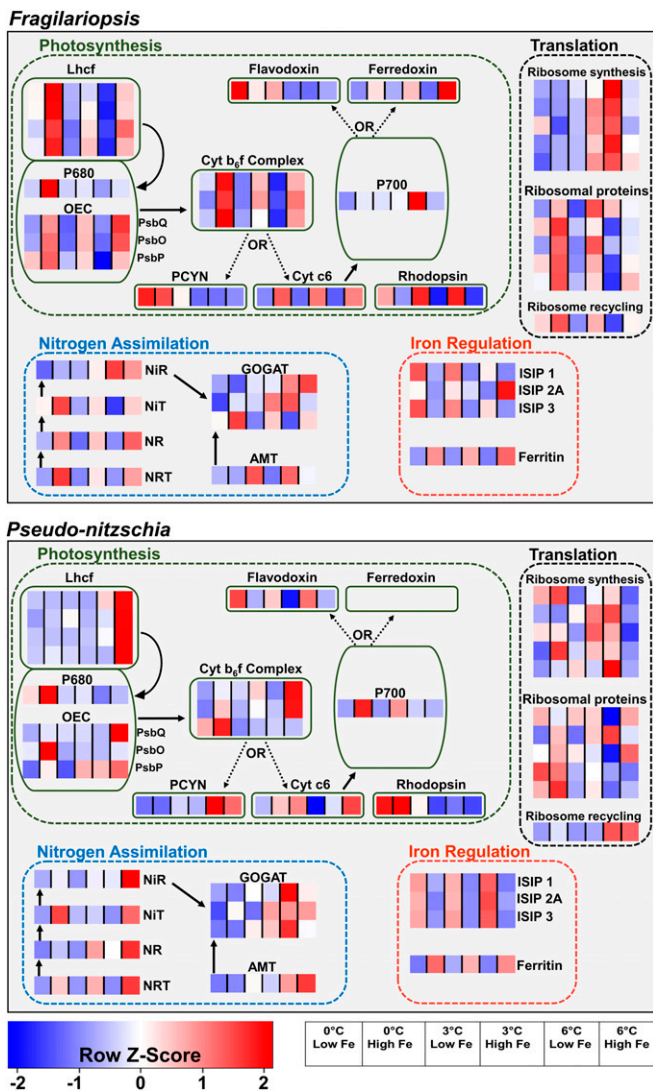


Fig. 2. Schematic representations of *Fragilariopsis* and *Pseudo-nitzschia* cells showing cellular processes, with each process comprised of several transcript clusters (MCL clusters). Photosynthesis: Lhcf = light harvesting complexes-f, OEC = oxygen evolving complex, Cyt b_6/f complex = cytochrome b_6/f complex, PCYN = plastocyanin, Cyt c6 = cytochrome c6. Nitrogen Assimilation: NRT = nitrate transporter, NR = nitrate reductase, NiT = nitrite transporter, NiR = nitrite reductase, AMT = ammonium transporter, GOGAT = glutamine oxoglutarate aminotransferase cycle. Iron Regulation: ISIP = iron starvation induced protein. Each row in a heatmap represents one MCL, each column represents a temperature and iron treatment at T5 with each block representing three biological replicate means with individual replicates shown in *SI Appendix, Fig. S9*. Heatmaps were constructed using taxon-normalized RPKM values. Empty heatmap placeholders represent clusters found in *Fragilariopsis* but not *Pseudo-nitzschia*. Arrows represent energy/electron flow in photosynthetic light reactions and steps involved in nitrogen assimilation using nitrate or ammonium.

account for up to 40% of cellular iron quotas (48) and are typically down-regulated under low iron (49, 50). Here, we did not detect the expression of iron-dependent electron acceptor ferredoxin (PetF) in *Pseudo-nitzschia*, regardless of iron status. Antarctic *Pseudo-nitzschia* species may have constitutively reduced dependence on PetF (51, 52) to minimize photosynthetic iron demand. **Light-Harvesting Complexes.** Most members of the light-harvesting complex (LHC) superfamily primarily absorb and direct light energy to photosynthetic reaction centers where charge separation

occurs, but some of them (Lhcx clade) are also involved in stress responses and photoprotection (53, 54). Expression patterns of transcripts belonging to the major Lhcf group and photosystem I (PSI)-associated Lhcr groups were markedly different between the two taxa under the different temperature and iron treatments (Fig. 4). In *Fragilariopsis*, there was a general pattern of decreased expression with warming and marked up-regulation with iron addition. In contrast, *Pseudo-nitzschia* showed a pattern of increasing expression with elevated temperatures. Up-regulation of Lhcf and Lhcr groups contributes to increased light harvesting efficiency and provides more energy for downstream temperature-dependent catalytic processes. This also alleviates photosynthetic iron demand by reducing the number of iron-containing photosynthetic components required to process light energy (55). Increased light harvesting cross-section has been measured under warming (3 °C and 6 °C compared to 1 °C) in iron-stressed *F. cylindrus* in the laboratory (14). However, these environmental data indicate that *Pseudo-nitzschia* may be even better equipped to use this mechanism to support growth under low iron in the SO, provided that the LHC up-regulation observed here reflects an increase in light harvesting cross-section, which remains speculative at this time. Several Lhcf and Lhcr clusters were also up-regulated in both *Fragilariopsis* and *Pseudo-nitzschia* after iron addition. Given that iron addition is expected to decrease light harvesting cross-section (13, 14, 56, 57), it might be predicted that iron addition could decrease the demand for Lhcf and Lhcr expression. However, this impact appears to be overridden by increased demand for LHC expression resulting from iron-induced increases in photosynthetic unit (PSU) abundance. Additional measurements of light absorption cross-section and photosynthetic efficiency could provide further insight into how light harvesting responds to changes in LHC expression under different iron and temperature conditions.

Each transcript cluster belonging to the Lhcx clade was down-regulated after 24 h of incubation at all temperatures and iron conditions in both *Fragilariopsis* and *Pseudo-nitzschia* (Fig. 4). Lhcx are highly sensitive to environmental change, including fluctuations in light and nutrient levels (53, 54, 58). Given these expression patterns and previous observations of Lhcx regulation, the Lhcx transcripts detected here may be responding to changes in the light levels that cells would have undergone during sample collection—brief exposure to unattenuated daylight during sampling, followed by lower light intensities in the incubations. Notably, expression of these Lhcx clades showed only minimal responses to iron addition.

Plastocyanin. Plastocyanin is a copper-containing protein that acts as an electron shuttle in the electron transport chain and plays an important role in reducing iron requirements in phytoplankton by substituting for cytochrome c_6 (12, 47, 59). Here, iron addition had no significant effect on plastocyanin transcript expression, while warming caused its up-regulation in *Pseudo-nitzschia* and down-regulation in *Fragilariopsis* (Fig. 3). Plastocyanin expression has been observed to be insensitive to iron availability in low-iron-adapted diatoms (43). However, our data suggest that *Pseudo-nitzschia* plastocyanin transcripts are phylogenetically distinct from those of *Fragilariopsis* and may play a temperature-responsive role to support growth under elevated temperatures (*SI Appendix, Fig. S6*). Plastocyanin transcript abundance in *Pseudo-nitzschia* was higher at 3 °C and 6 °C compared to -0.5 °C at T1, showing a rapid response to warming (*SI Appendix, Fig. S6*). This, in combination with the strong and immediate response of LHCs may give *Pseudo-nitzschia* a photosynthetic advantage over *Fragilariopsis* across a wide range of likely warming scenarios in the SO.

Nitrogen Metabolism. KO term enrichment analysis showed that transcripts encoding nitrogen metabolism were enriched in *Pseudo-nitzschia* and depleted in *Fragilariopsis* after temperature

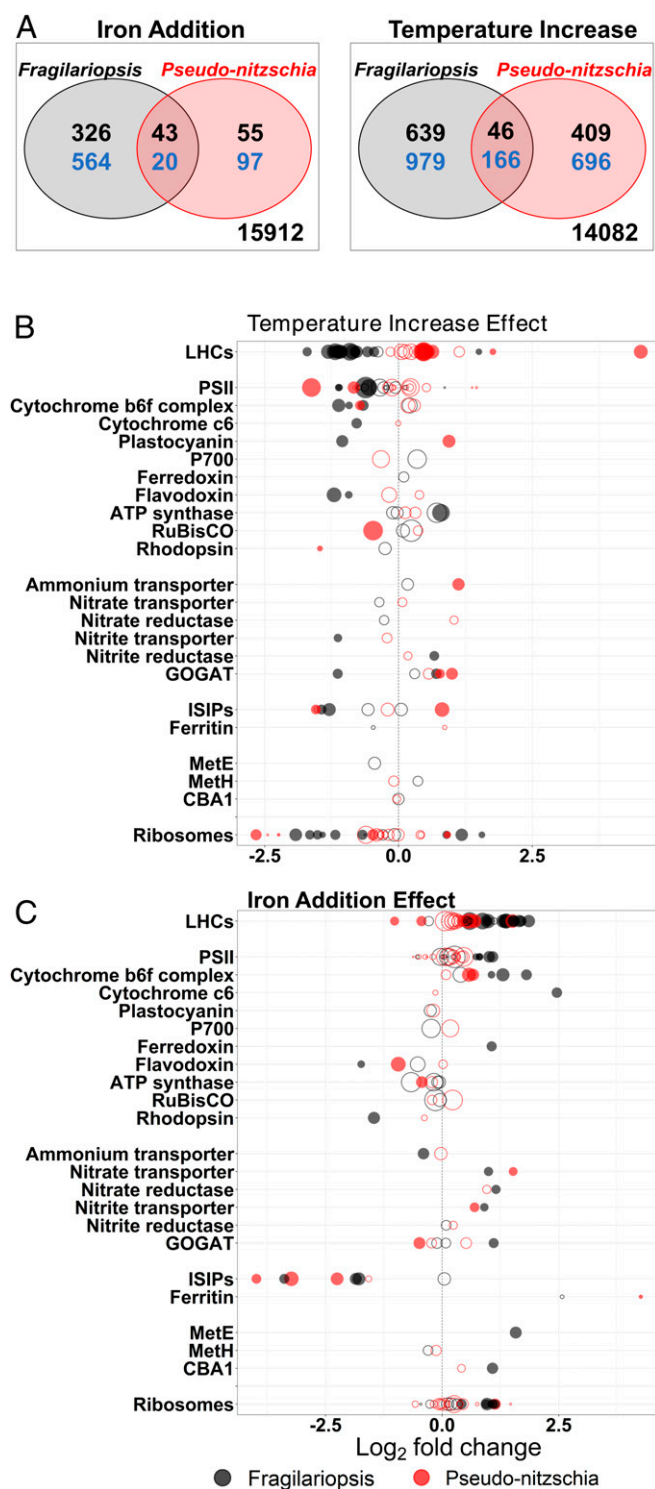


Fig. 3. (A) Venn diagram showing the number of transcript clusters that are significantly up- (black) or down- (blue) regulated with iron addition or temperature increase in *Fragilariopsis* and *Pseudo-nitzschia*. The intersection represents clusters up- or down-regulated in both *Fragilariopsis* and *Pseudo-nitzschia*. The number outside of the circles represents the number of clusters from both taxa that were not differentially expressed. In both taxa, warming caused more clusters to be differentially expressed than iron addition. (B) Differential expression (DE) of various clusters under increased temperature. DE was calculated using the quasi-likelihood test (glmQLFTest) in EdgeR, and fold change was calculated for high-temperature (6 °C) versus low-temperature (−0.5 °C) treatments at T5. (C) DE of various clusters after iron addition. DE was calculated using the quasi-likelihood test (glmQLFTest)

increase (*SI Appendix*, Figs. S4 and S5). Nitrogen is required for protein synthesis and would be necessary to support the observed increase in *Pseudo-nitzschia* cell counts under warming, and notably, dissolved nitrogen drawdown was enhanced due to warming alone and elevated further upon iron addition (Fig. 5 A and B). However, nitrogen acquisition and assimilation from nitrate requires iron (60), and the observed *Pseudo-nitzschia* growth under elevated temperature would necessitate iron-economic nitrogen metabolism. Our data show that ammonium transporter transcripts were up-regulated in *Pseudo-nitzschia* but not in *Fragilariopsis* under warming (Figs. 3B and 5 C and D), indicating that *Pseudo-nitzschia* is better equipped to utilize ammonium as an additional and/or alternative nitrogen source in response to elevated nitrogen demand, which is likely a result of increased growth in response to warming. Elevated ammonium transporter expression would provide *Pseudo-nitzschia* with an additional nitrogen source at a lower iron cost for use in amino acid synthesis and growth (60–62). In fact, community ammonium drawdown at 6 °C was greater than at lower temperatures, regardless of iron status (Fig. 5B), consistent with the notion that ammonium use at high temperature and low iron could have contributed to the success of *Pseudo-nitzschia*. The ability to uptake and utilize ammonium rapidly, relative to nitrate, also allows diatoms to grow faster when ammonium is available (63, 64). However, the high *Pseudo-nitzschia* growth we observed cannot be supported by ammonium alone; total community ammonium drawdown comprised only $25.2 \pm 2.4\%$ of dissolved inorganic nitrogen (nitrate + ammonium) drawdown in the 6 °C no added iron treatment and $7.9 \pm 1.0\%$ of dissolved inorganic nitrogen drawdown in the added iron 6 °C treatment (Fig. 5 A and B). Nitrate drawdown was responsible for the majority of dissolved nitrogen uptake regardless of iron status, though significantly (two-way ANOVA, $P = 9.6 \times 10^{-11}$) more so under elevated iron. This suggests that *Pseudo-nitzschia* may have utilized additional parsimonious mechanisms such as internal protein recycling to further reduce nitrogen requirements and thereby reduce iron demand (65). While nitrate drawdown was elevated at high temperatures both with and without added iron (Fig. 5A), neither *Pseudo-nitzschia* nor *Fragilariopsis* changed their expression of nitrate transporters in response to elevated temperature. Both diatom groups up-regulated nitrate transporters in response to iron addition regardless of temperature (Figs. 3 and 5 E and F). Similarly, nitrate reductase transcript expression was up-regulated in response to iron addition but not elevated temperature (Figs. 3 and 5 G and H). However, the observed elevation in nitrate drawdown and nitrate uptake rates with warming (Figs. 1 and 5), in the absence of a change in gene expression, is consistent with the well-characterized temperature dependence of nitrate reductase activity (26). This suggests that the enhanced nitrate assimilation under elevated temperature was indeed accomplished without the increase in iron demand required to produce additional copies of active nitrate reductase.

Genetic Information Processing/Translation. Protein synthesis is an energetically costly process that is required for metabolism and growth. Increased kinetic energy due to warming enhances translation efficiency, reduces the total RNA per cell, and reduces the number of ribosomes required to maintain protein synthesis rates (66). Consistent with this response, we observed that several

in EdgeR, and fold change was calculated for iron-added versus no iron-added treatments at T5. In both B and C, positive and negative Log₂ fold change values represent up- and down-regulation, respectively. Filled circles are clusters with statistically significant DE (adjusted *P* value < 0.05). Point size represents total normalized transcript abundance under all iron and temperature treatments.

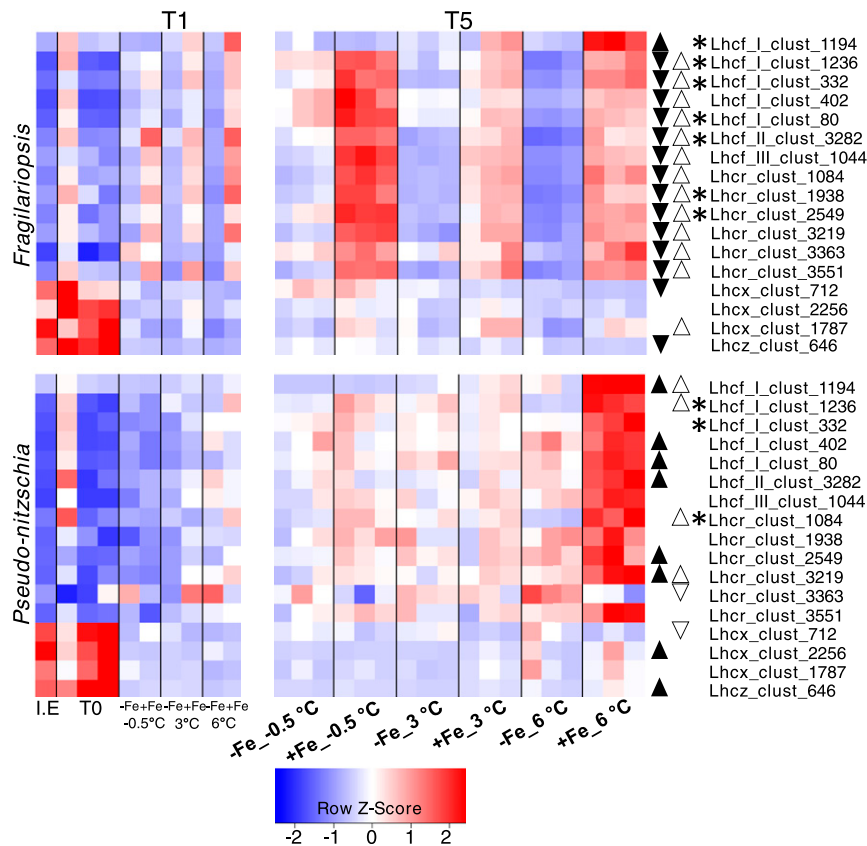


Fig. 4. Heatmaps of MCL clusters of LHCs Lhcf, Lhcr, Lhcx, and Lhcz (reference *SI Appendix, Table S6*) in *Pseudo-nitzschia* and *Fragilariopsis* measured after 24 h (T1) and 5 d (T5) of incubation under the various iron and temperature treatments. Heatmaps were constructed using taxon-normalized RPKM values. I.E represents IE samples; T0 represents in situ samples processed immediately before any incubations. Each block is one biological replicate measurement. Black and white up/down pointing triangles represent transcripts that were significantly (glmQLFTest-EdgeR $P < 0.05$) up- or down-regulated due to warming or iron addition (respectively) at T5. Stars represent transcripts that were significantly (glmQLFTest-EdgeR $P < 0.05$) up-regulated due to an interactive iron-temperature effect at T5.

transcript clusters corresponding to ribosomes were down-regulated in both *Fragilariopsis* and *Pseudo-nitzschia* under warming (Figs. 2 and 3). Warming also caused up-regulation of transcripts encoding ribosomal recycling proteins only in *Pseudo-nitzschia* (Fig. 2), which can reduce nitrogen demand and the energetic costs associated with ribosomal synthesis. While the reduction in phosphorus-rich ribosome abundance is thought to increase cellular N:P ratios, leading to increased nitrogen demand in warmer ocean regions (66), our bulk nutrient drawdown ratios (*SI Appendix, Fig. S1*) show that N:P drawdown is not significantly influenced by warming (two-way ANOVA, $P = 0.07$). This suggests that the increasing dominance of diatoms, with their considerably lower N:P ratios than other SO plankton groups such as *Phaeocystis* (22, 67), is likely an overall driver of N:P ratios and can counterbalance the expected reduction in cellular phosphate demand at high temperature from reduced ribosome content. It is also possible that temperature changes alone, without additional interactive effects due to changes in other variables such as CO₂ and light, might not cause a strong increase in N:P ratios (68).

Micronutrient Acquisition, Trafficking, and Storage. Increased iron uptake, storage, and intracellular transport are strategies to improve growth under low iron availability. In the laboratory, Zhu et al. (22) report higher iron uptake rates in *P. subcurvata* than in *F. cylindrus* under warming. Our data show down-regulation of iron stress-induced proteins (ISIP1, ISIP2A, ISIP3) in both *Pseudo-nitzschia* and *Fragilariopsis* after iron addition, and ISIP2A up-regulation only in *Pseudo-nitzschia* after warming (Figs. 2 and 3).

ISIPs are involved in iron acquisition and storage systems in diatoms, and specifically, ISIP2A contributes to nonreductive iron uptake (16–18, 50). No previous studies have inspected ISIP2A response to temperature, but it is likely that the apparent temperature response of ISIP2A contributes to the ability of *Pseudo-nitzschia* to acquire and utilize iron to support growth under warming. Additionally, transcripts for ferritin, an iron storage protein (19), were significantly up-regulated only in *Pseudo-nitzschia* after iron addition (Fig. 3). Several studies have reported ferritin up-regulation in *Pseudo-nitzschia* under iron-replete conditions (44, 69), and *Fragilariopsis* can also utilize ferritin to store iron (19). However, consistent with low *Fragilariopsis* ferritin expression under iron-replete conditions in the field (70), our study shows that *Fragilariopsis* ferritin transcripts were not significantly up-regulated after iron addition (Fig. 3). These trends suggest that in addition to reducing iron demand, *Pseudo-nitzschia* was better able to increase iron uptake and utilized stored ferritin-bound iron to support growth under warming. This suggests that *Pseudo-nitzschia* may be particularly well suited to environments with episodic iron availability.

In addition to iron, cobalamin has also been shown to be a critical micronutrient driver of phytoplankton growth and community composition in the SO (39). *Fragilariopsis* and *Pseudo-nitzschia*'s cobalamin acquisition and stress response machinery also showed markedly different responses to iron and warming (Fig. 3 and *SI Appendix, Fig. S7*), suggesting that these two diatoms may employ different strategies to cope with low cobalamin availability (*SI Appendix, Supplemental Results and Discussion*).

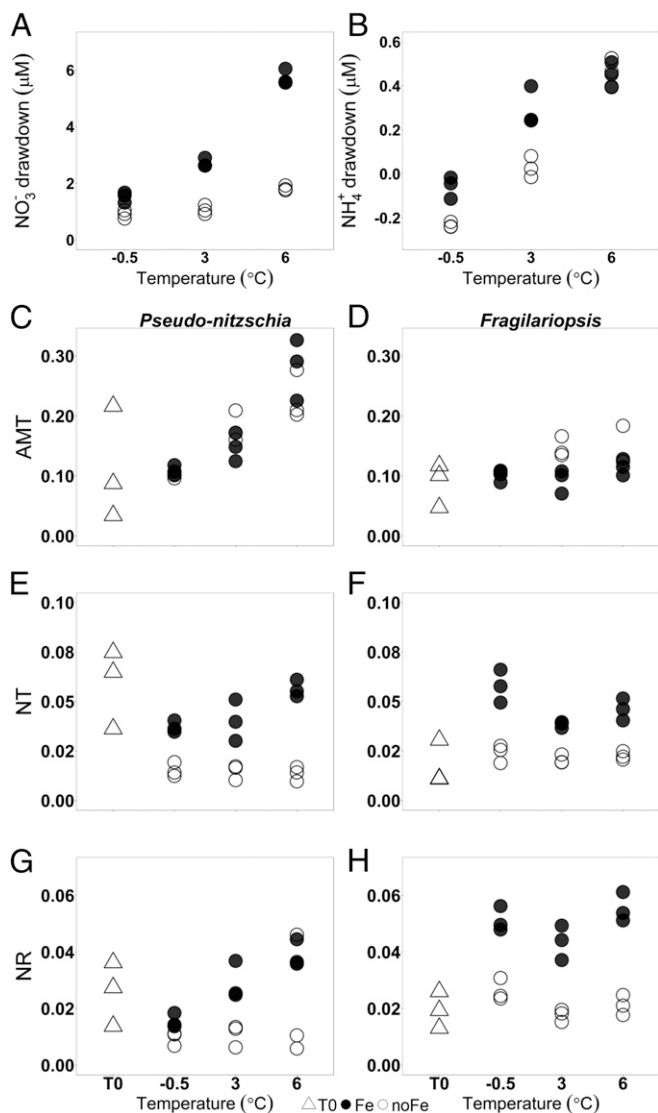


Fig. 5. (A and B) Total nitrate and ammonium drawdown from beginning to end of the experiment (difference in concentration between T7 and T0). (C–H) Taxon-normalized RPKM expression values for clusters belonging to ammonium transporters (AMT), nitrate transporters (NT), and nitrate reductase (NR) in both *Pseudo-nitzschia* and *Fragilariopsis* prior to incubation (T0) and at T5 with and without added iron at -0.5 , 3 , and 6 °C.

Synergistic Responses and Gene Expression. The observed synergistic iron–temperature effects on growth and nutrient drawdown were not accompanied by a synergistic effect on gene expression (SI Appendix, Figs. S3 and S10). For example, we did not observe an interactive iron–temperature effect on the expression of genes involved in nitrogen uptake, yet nitrate and ammonium drawdown increased synergistically due to iron and temperature increase (Fig. 1). It is unlikely that synergistic nutrient drawdown was influenced by synergistic gene expression in taxa other than *Fragilariopsis* and *Pseudo-nitzschia*. Except for the prokaryotic Alteromonadales group, we observed relatively little or no interactive iron–temperature effect on gene expression in all the taxa we assessed (SI Appendix, Fig. S3). This suggests that improved enzymatic efficiency under warming can accelerate metabolic functions, even without a proportional increase in transcript abundance. It is worth noting that, without extensive genetic manipulation and biochemical investigations using monocultures in

controlled conditions, observational studies like this lack the ability to disentangle causal relationships between gene expression patterns and physiology/growth. Nevertheless, observations of gene expression trends under different environmental conditions provide insight into the cellular mechanisms that facilitate growth and those which underpin differences between ecologically important groups.

Ecological and Biogeochemical Relevance. Most recent model projections show warming trends across the SO with sea surface temperatures increasing by 1 to 2 °C by 2100 and ~ 6 °C by 2300 (2, 4, 71). *Fragilariopsis* grows in a wide range of environments throughout the SO but is most successful in high-salinity, high-iron sea ice while *Pseudo-nitzschia* is most successful in warmer low-salinity, low-iron meltwaters (33, 72, 73). The growth and gene expression patterns we observed in both diatoms may then be driven by niche-specific adaptations due to competition for resources. Our results are consistent with a 2013 incubation study conducted at the IE in the Ross Sea where *Pseudo-nitzschia* dominated the community after warming (28), suggesting that Antarctic *Pseudo-nitzschia* are better equipped to dominate in a warmer (4 °C compared to 0 °C) ocean and even more so if iron availability increases. A shift into a *Pseudo-nitzschia* dominated community raises concerns for domoic acid (DA) production and its toxic effects in mammals and other trophic levels (74, 75). A search for DA biosynthesis transcripts (76) did not yield strong evidence for expression of the DA biosynthesis gene cluster in this experiment (SI Appendix, Tables S4 and S5). However, other studies have measured DA concentrations as high as 220 ng L⁻¹ in the SO (77, 78), but the temporal, spatial, and environmental factors that elicit DA production remain unclear. Further work is required to investigate whether resident *Pseudo-nitzschia* can produce the toxin under conditions not examined in our study or if DA producing *Pseudo-nitzschia* are likely to migrate into a warmer SO.

A change in SO phytoplankton community structure could have important biogeochemical ramifications on local and global scales. Changes in cell size, frustule thickness, and metabolic functions under changing temperature and iron conditions could influence ecosystem and biogeochemical processes by altering sinking rates, grazing pressures, and cellular nutrient quotas (37, 42, 68). Warming-induced increases in the expression of ISIP2A, as well as iron-conserving plastocyanin, LHCs, and nitrogen assimilation processes suggest the involvement of a suite of mechanisms that support growth under warming. These cellular changes resulted in increased nutrient drawdown in our multiday experiment, even in the face of iron limitation. Such warming-enhanced SO nutrient drawdown could have profound consequences for northward nutrient supply, especially if cells are able to utilize these parsimonious processes over weeks or months and if the trends we observe in this coastal experiment hold true across broad swaths of the SO. As more nutrients such as nitrogen and phosphorous are consumed by phytoplankton and exported out of the surface ocean around Antarctica, less nutrients will be available to fuel productivity at lower latitudes (2). Here, we have identified molecular mechanisms that appear to enable diatoms, particularly *Pseudo-nitzschia*, to accomplish enhanced growth and nutrient drawdown with rising temperatures under low-iron conditions. These mechanisms, up-regulation of iron-conserving photosynthetic processes, utilization of iron-economic nitrogen assimilation mechanisms, and increased iron uptake and storage, underpin what may be a pattern of increasing nutrient utilization in the SO and decreasing availability of nutrients for lower latitudes.

Materials and Methods Summary

Seawater was collected at a 3-m depth at the IE from McMurdo Sound, Antarctica on January 15, 2015 ($165^{\circ}24.7985^{\circ}\text{E}$, $77^{\circ}37.1370^{\circ}\text{S}$) using previously

described trace-metal-clean techniques (39). Triplicate bottles of each treatment (temperature: $-0.5\text{ }^{\circ}\text{C} \pm 0.2\text{ }^{\circ}\text{C}$, $3 \pm 0.5\text{ }^{\circ}\text{C}$, and $6 \pm 0.5\text{ }^{\circ}\text{C}$; iron: not added [$+0\text{ nM}$], added [$+2\text{ nM}$]) were incubated indoors at a constant irradiance of 65 to 85 $\mu\text{E m}^{-2}\text{ sec}^{-1}$. This incubation irradiance is generally growth saturating for Antarctic phytoplankton (57, 79) and falls within observational bounds of mean mixed layer light levels (80, 81). Metatranscriptome samples were taken at the sea IE, in the laboratory immediately following bottle incubation setup (T0), on January 16 (T1), and again on January 20 (T5). Cell counts were measured on T0 and January 22 (T7). Dissolved nutrients (nitrate, phosphate, silicate) were measured on T0, T1, T3, T5, and T7, and ammonium was measured on T0 and T7. Primary productivity (bicarbonate uptake) and nitrate uptake rates were measured on T0, T1, T3, and T7 (SI Appendix, Fig. S1).

For metatranscriptomics, the microbial community was harvested on 0.2- μm Sterivex filters, total RNA was extracted using TRIzol reagent (Thermo Fisher Scientific), and ribosomal RNA was removed with Ribo-Zero Magnetic kits (Illumina). The resulting messenger RNA (mRNA) was purified and subjected to amplification and complementary DNA (cDNA) synthesis, using the Ovation RNA-Seq System V2 (TECAN). One microgram of the resulting cDNA pool was fragmented to a mean length of 200 base pairs, and libraries were prepared using Truseq kit (Illumina) and subjected to paired-end sequencing via Illumina HiSeq. Illumina paired reads were filtered to eliminate primer sequences and quality trimmed to Phred Q33, and rRNA was identified and removed using riboPicker (82). Transcript contigs were assembled de novo using CLC Assembly Cell (<https://www.qiagenbioinformatics.com/>), and ORFs were predicted using FragGeneScan (83). ORFs were annotated for putative function using hidden Markov models and BLAST-p against PhyloDB (39) and filtered to eliminate those with low mapping coverage (<50 reads total over all samples) and proteins with no BLAST hits and no known domains. ORFs were assigned to taxonomic groups of interest (SI Appendix, Fig. S2) based on best Lineage Probability Index (LPI) taxonomy (39, 84). Reads per kilobase mapped (RPKM) expression values for each ORF were calculated and taxon normalized using a normalization factor representing the summed taxonomic group contribution to total nuclear-assigned reads per sample. ORFs were clustered into orthologs and protein families using MCL (46). Group normalized cluster (average/total) RPKM expression values were calculated by pooling the taxon-normalized expression values for each group within a cluster. Cluster annotations were aggregated by annotation type (KEGG, KO, euKaryotic Orthologous Groups [KOG], KOG class, Pfam, TIGRfam, Enzyme Commission [EC], Gene Ontology [GO]), and a single annotation was chosen to represent each cluster based on the lowest Fisher's exact test P value (fisher.test in R).

Differential gene expression at T5 (foldchange magnitude and adjusted P value) was calculated using empirical Bayes quasi-likelihood F-tests (glmQLFTest

in edgeR) on taxon-normalized expression values to account for the change in abundance under the different iron and temperature treatments. A P value cut off of 0.05 was used for statistical significance. Iron effect was determined by comparing all $-Fe$ treatments at T5 to all $+Fe$ treatments at T5. Temperature effect was determined by comparing all $-0.5\text{ }^{\circ}\text{C}$ to $3\text{ }^{\circ}\text{C}$ treatments at T5 and $-0.5\text{ }^{\circ}\text{C}$ to $6\text{ }^{\circ}\text{C}$ at T5. A gene was considered up-regulated with temperature if it was up-regulated in both $-0.5\text{ }^{\circ}\text{C}$ versus $3\text{ }^{\circ}\text{C}$ and $-0.5\text{ }^{\circ}\text{C}$ versus $6\text{ }^{\circ}\text{C}$ tests.

Stable isotope tracer techniques, using ^{15}N -labeled nitrate and ^{13}C -labeled bicarbonate (Cambridge Isotope Laboratories), were used to determine uptake rates, similar to methods previously described in Ross Sea nutrient utilization studies (28). Tracer amounts of labeled substrates were added to bottles containing the initial IE community (T0) and to subsampled volume from treatments at T1, T3, and T7. After incubations ($\sim 6\text{ h}$), the microbial communities ($>0.7\text{ }\mu\text{m}$) were collected on glass fiber filters (Whatman GF/F; combusted at $450\text{ }^{\circ}\text{C}$ for 2 h) and stored frozen. Isotopic enrichments of ^{15}N and ^{13}C were measured on a Europa 20/20 isotope ratio mass spectrometer, and absolute uptake rates ($\mu\text{M h}^{-1}$) were calculated according to ref. 85. Complete methods and uptake rate measurements from all time points can be found in SI Appendix, Fig. S1.

Data Availability. The data reported in this paper have been deposited in the National Center for Biotechnology Information sequence read archive (BioProject accession no. PRJNA637767; RNA-Seq BioSample accession nos. SAMN15154229–SAMN15154256, 18S ribosomal RNA (rRNA) amplicon BioSample accession nos. SAMN18528738–SAMN18528777). Contigs, assembled ORFs, 18S rRNA abundance, and MCL cluster abundance and differential expression analysis results are available at: <http://datadryad.org/stash/dataset/doi:10.5061/dryad.qjskxsn3j> (86).

ACKNOWLEDGMENTS. We are grateful to Antarctic Support Contractors, especially Ned Corkran, for facilitating fieldwork. We thank Jeff Hoffman, Zhi Zhu, and Quinn Roberts for assistance in the field, Hong Zheng for her work in the laboratory, and Pratap Venepally for assistance with bioinformatic analyses. This study was funded by NSF Antarctic Sciences Awards 1103503 (to E.M.B.), 0732822 and 1043671 (to A.E.A.), 1043748 (to D.A.H.), 1043635 (to D.A.B.); Gordon and Betty Moore Foundation Grant GBMF3828 (to A.E.A.); NSF Ocean Sciences Award NSF-OCE-1136477 and NSF-OCE-1756884 (to A.E.A.) and NSF-OCE-1638804 and NSF-OCE-1851222 (to D.A.H.); Nova Scotia Graduate Scholarship to L.J.J.; National Sciences and Engineering Research Council of Canada - Canada Graduate Scholarship and Transatlantic Ocean System Science & Technology scholarship to J.S.P.M.; NSERC Discovery Grant RGPIN-2015-05009 to E.M.B.; Simons Foundation Grant 504183 to E.M.B.; and Canada Research Chair support to E.M.B.

1. T. L. Frölicher *et al.*, Dominance of the Southern Ocean in anthropogenic carbon and heat uptake in CMIP5 models. *J. Clim.* **28**, 862–886 (2015).
2. J. K. Moore *et al.*, Sustained climate warming drives declining marine biological productivity. *Science* **359**, 1139–1143 (2018).
3. J. Turner *et al.*, Antarctic climate change during the last 50 years. *Int. J. Climatol.* **25**, 279–294 (2005).
4. P. W. Boyd, S. T. Lennartz, D. M. Glover, S. C. Doney, Biological ramifications of climate-change-mediated oceanic multi-stressors. *Nat. Clim. Chang.* **5**, 71–79 (2015).
5. IPCC, IPCC special report on the ocean and cryosphere in a changing climate (2019). <https://www.ipcc.ch/srocc/>. Accessed 9 July 2021.
6. A. Tagliabue *et al.*, How well do global ocean biogeochemistry models simulate dissolved iron distributions? *Global Biogeochem. Cycles* **30**, 149–174 (2016).
7. D. A. Hutchins, P. W. Boyd, Marine phytoplankton and the changing ocean iron cycle. *Nat. Clim. Chang.* **6**, 1072–1079 (2016).
8. R. Eppley, Temperature and phytoplankton growth in the sea. *Fish Bull.* **70**, 1063–1085 (1972).
9. J. H. Martin, S. E. Fitzwater, R. M. Gordon, Iron deficiency limits phytoplankton growth in Antarctic waters. *Global Biogeochem. Cycles* **4**, 5–12 (1990).
10. H. de Baar *et al.*, On iron limitation of the Southern Ocean: Experimental observations in the Weddell and Scotia Seas. *Mar. Ecol. Prog. Ser.* **65**, 105–122 (1990).
11. A. Pankowski, A. McMinn, Iron availability regulates growth, photosynthesis, and production of ferredoxin and flavodoxin in Antarctic sea ice diatoms. *Aquat. Biol.* **4**, 273–288 (2009).
12. G. Peers, N. M. Price, Copper-containing plastocyanin used for electron transport by an oceanic diatom. *Nature* **441**, 341–344 (2006).
13. R. F. Strzepek, P. W. Boyd, W. G. Sunda, Photosynthetic adaptation to low iron, light, and temperature in Southern Ocean phytoplankton. *Proc. Natl. Acad. Sci. U.S.A.* **116**, 4388–4393 (2019).
14. L. Jabre, E. M. Bertrand, Interactive effects of iron and temperature on the growth of *Fragilariopsis cylindrus*. *Limnol. Oceanogr. Lett.* **5**, 363–370 (2020).
15. A. Marchetti, D. Catlett, B. M. Hopkinson, K. Ellis, N. Cassar, Marine diatom proteorhodopsins and their potential role in coping with low iron availability. *ISME J.* **9**, 2745–2748 (2015).
16. J. Morrissey *et al.*, A novel protein, ubiquitous in marine phytoplankton, concentrates iron at the cell surface and facilitates uptake. *Curr. Biol.* **25**, 364–371 (2015).
17. E. Kazamia *et al.*, Endocytosis-mediated siderophore uptake as a strategy for Fe acquisition in diatoms. *Sci. Adv.* **4**, eaar4536 (2018).
18. J. B. McQuaid *et al.*, Carbonate-sensitive phytoferrotransferrin controls high-affinity iron uptake in diatoms. *Nature* **555**, 534–537 (2018).
19. A. Marchetti *et al.*, Ferritin is used for iron storage in bloom-forming marine pennate diatoms. *Nature* **457**, 467–470 (2009).
20. J. A. Raven, R. J. Geider, Temperature and algal growth. *New Phytol.* **110**, 441–461 (1988).
21. J. M. Rose *et al.*, Synergistic effects of iron and temperature on Antarctic phytoplankton and microzooplankton assemblages. *Biogeosciences* **6**, 3131–3147 (2009).
22. Z. Zhu *et al.*, A comparative study of iron and temperature interactive effects on diatoms and *Phaeocystis antarctica* from the Ross Sea, Antarctica. *Mar. Ecol. Prog. Ser.* **550**, 39–51 (2016).
23. W. G. Sunda, S. A. Huntsman, Interactive effects of light and temperature on iron limitation in a marine diatom: Implications for marine productivity and carbon cycling. *Limnol. Oceanogr.* **56**, 1475–1488 (2011).
24. H.-B. Jiang *et al.*, Ocean warming alleviates iron limitation of marine nitrogen fixation. *Nat. Clim. Chang.* **8**, 709–712 (2018).
25. N. Yang *et al.*, Warming iron-limited oceans enhance nitrogen fixation and drive biogeographic specialization of the globally important cyanobacterium *Crocosphaera*. *Front. Mar. Sci.* **8**, 1–11 (2021).
26. Y. Gao, G. J. Smith, R. S. Alberte, Temperature dependence of nitrate reductase activity in marine phytoplankton: Biochemical analysis and ecological implications. *J. Phycol.* **36**, 304–313 (2001).
27. V. M. di Rigano *et al.*, Temperature dependence of nitrate reductase in the psychrophilic unicellular alga *Koliella antarctica* and the mesophilic alga *Chlorella sorokiniana*. *Plant Cell Environ.* **29**, 1400–1409 (2006).
28. J. Spackee *et al.*, Impact of temperature, CO_2 , and iron on nutrient uptake by a late-season microbial community from the Ross Sea, Antarctica. *Aquat. Microb. Ecol.* **82**, 145–159 (2018).
29. P. W. Boyd, Physiology and iron modulate diverse responses of diatoms to a warming Southern Ocean. *Nat. Clim. Chang.* **9**, 148–152 (2019).

30. S. M. Andrew, H. T. Morell, R. F. Strzepek, P. W. Boyd, M. J. Ellwood, Iron availability influences the tolerance of southern ocean phytoplankton to warming and elevated irradiance. *Front. Mar. Sci.* **6**, 1–12 (2019).
31. P. Boyd, D. Hutchins, Understanding the responses of ocean biota to a complex matrix of cumulative anthropogenic change. *Mar. Ecol. Prog. Ser.* **470**, 125–135 (2012).
32. D. A. Hutchins *et al.*, Control of phytoplankton growth by iron and silicic acid availability in the subantarctic Southern Ocean: Experimental results from the SAZ project. *J. Geophys. Res.* **106**, 31559–31572 (2001).
33. O. Sackett *et al.*, Phenotypic plasticity of southern ocean diatoms: Key to success in the sea ice habitat? *PLoS One* **8**, e81185 (2013).
34. A. Coello-Camba, S. Agustí, Thermal thresholds of phytoplankton growth in polar waters and their consequences for a warming polar ocean. *Front. Mar. Sci.* **4**, 168 (2017).
35. P. Tréguer *et al.*, Influence of diatom diversity on the ocean biological carbon pump. *Nat. Geosci.* **11**, 27–37 (2018).
36. C. Laufkötter *et al.*, Drivers and uncertainties of future global marine primary production in marine ecosystem models. *Biogeosciences* **12**, 6955–6984 (2015).
37. P. Assmy *et al.*, Thick-shelled, grazer-protected diatoms decouple ocean carbon and silicon cycles in the iron-limited Antarctic circumpolar current. *Proc. Natl. Acad. Sci. U.S.A.* **110**, 20633–20638 (2013).
38. K. R. Arrigo, G. L. van Dijken, S. Bushinsky, Primary production in the Southern Ocean, 1997–2006. *J. Geophys. Res.* **113**, 10.1029/2007JC004551 (2008).
39. E. M. Bertrand *et al.*, Phytoplankton-bacterial interactions mediate micronutrient colimitation at the coastal Antarctic sea ice edge. *Proc. Natl. Acad. Sci. U.S.A.* **112**, 9938–9943 (2015).
40. O. Mangoni *et al.*, Phytoplankton blooms during austral summer in the Ross Sea, Antarctica: Driving factors and trophic implications. *PLoS One* **12**, e0176033 (2017).
41. S.-H. Kang, G. A. Fryxell, *Fragilariopsis cylindrus* (Grunow) Krieger: The most abundant diatom in water column assemblages of Antarctic marginal ice-edge zones. *Polar Biol.* **12**, 609–627 (1992).
42. B. Quéguiner, Iron fertilization and the structure of planktonic communities in high nutrient regions of the Southern Ocean. *Deep Sea Res. Part II Top. Stud. Oceanogr.* **90**, 43–54 (2013).
43. A. Marchetti *et al.*, Comparative metatranscriptomics identifies molecular bases for the physiological responses of phytoplankton to varying iron availability. *Proc. Natl. Acad. Sci. U.S.A.* **109**, E317–E325 (2012).
44. N. R. Cohen *et al.*, Transcriptomic and proteomic responses of the oceanic diatom *Pseudo-nitzschia granii* to iron limitation. *Environ. Microbiol.* **20**, 3109–3126 (2018).
45. R. P. Kiene, D. Slezak, Low dissolved DMSP concentrations in seawater revealed by small-volume gravity filtration and dialysis sampling: Filtration and dialysis for dissolved DMSP. *Limnol. Oceanogr. Methods* **4**, 80–95 (2006).
46. A. J. Enright, S. Van Dongen, C. A. Ouzounis, An efficient algorithm for large-scale detection of protein families. *Nucleic Acids Res.* **30**, 1575–1584 (2002).
47. M. Wu *et al.*, Manganese and iron deficiency in Southern Ocean *Phaeocystis antarctica* populations revealed through taxon-specific protein indicators. *Nat. Commun.* **10**, 3582 (2019).
48. J. A. Raven, M. C. W. Evans, R. E. Korb, The role of trace metals in photosynthetic electron transport in O₂-evolving organisms. *Photosynth. Res.* **60**, 111–149 (1999).
49. J. LaRoche, P. W. Boyd, M. McKay, R. Geider, Flavodoxin as an in situ marker for iron stress in phytoplankton. *Nature* **382**, 802–805 (1996).
50. A. E. Allen *et al.*, Whole-cell response of the pennate diatom *Phaeodactylum tricorutum* to iron starvation. *Proc. Natl. Acad. Sci. U.S.A.* **105**, 10438–10443 (2008).
51. A. Pankowski, A. McMinn, Development of immunoassays for the iron-regulated proteins Ferredoxin and Flavodoxin in polar microalgae. *J. Phycol.* **45**, 771–783 (2009).
52. C. M. Moreno *et al.*, Examination of gene repertoires and physiological responses to iron and light limitation in Southern Ocean diatoms. *Polar Biol.* **41**, 679–696 (2018).
53. S.-H. Zhu, B. R. Green, Photoprotection in the diatom *Thalassiosira pseudonana*: Role of L1818-like proteins in response to high light stress. *Biochim. Biophys. Acta* **1797**, 1449–1457 (2010).
54. J. M. Buck *et al.*, Lhcx proteins provide photoprotection via thermal dissipation of absorbed light in the diatom *Phaeodactylum tricorutum*. *Nat. Commun.* **10**, 4167 (2019).
55. N. Schuback, C. Schallenberg, C. Duckham, M. T. Maldonado, P. D. Tortell, Interacting effects of light and iron availability on the coupling of photosynthetic electron transport and CO₂-assimilation in marine phytoplankton. *PLoS One* **10**, e0133235 (2015).
56. R. M. Greene, R. J. Geider, Z. Kolber, P. G. Falkowski, Iron-induced changes in light harvesting and photochemical energy conversion processes in eukaryotic marine algae. *Plant Physiol.* **100**, 565–575 (1992).
57. R. F. Strzepek, K. A. Hunter, R. D. Frew, P. J. Harrison, P. W. Boyd, Iron-light interactions differ in Southern Ocean phytoplankton. *Limnol. Oceanogr.* **57**, 1182–1200 (2012).
58. L. Taddei *et al.*, Multisignal control of expression of the LHCX protein family in the marine diatom *Phaeodactylum tricorutum*. *J. Exp. Bot.* **67**, 3939–3951 (2016).
59. J. A. Raven, Iron acquisition and allocation in stramenopile algae. *J. Exp. Bot.* **64**, 2119–2127 (2013).
60. H. Schoffman, H. Lis, Y. Shaked, N. Keren, Iron-nutrient interactions within phytoplankton. *Front. Plant Sci.* **7**, 1–12 (2016).
61. J. A. Raven, The iron and molybdenum use efficiencies of plant growth with different energy, carbon and nitrogen sources. *New Phytol.* **109**, 279–287 (1988).
62. S. R. Smith *et al.*, Evolution and regulation of nitrogen flux through compartmentalized metabolic networks in a marine diatom. *Nat. Commun.* **10**, 4552 (2019).
63. J. S. Parslow, P. J. Harrison, P. A. Thompson, Development of rapid ammonium uptake during starvation of batch and chemostat cultures of the marine diatom *Thalassiosira pseudonana*. *Mar. Biol.* **83**, 43–50 (1984).
64. K. Tada *et al.*, Diatoms grow faster using ammonium in rapidly flushed eutrophic Dokai Bay, Japan. *J. Oceanogr.* **65**, 885–891 (2009).
65. B. L. Nunn *et al.*, Diatom proteomics reveals unique acclimation strategies to mitigate Fe limitation. *PLoS One* **8**, e75653 (2013).
66. A. Toseland *et al.*, The impact of temperature on marine phytoplankton resource allocation and metabolism. *Nat. Clim. Chang.* **3**, 979–984 (2013).
67. K. R. Arrigo *et al.*, Phytoplankton community structure and the drawdown of nutrients and CO₂ in the southern ocean. *Science* **283**, 365–367 (1999).
68. P. W. Boyd *et al.*, Physiological responses of a Southern Ocean diatom to complex future ocean conditions. *Nat. Clim. Chang.* **6**, 207–213 (2016).
69. N. R. Cohen *et al.*, Iron storage capacities and associated ferritin gene expression among marine diatoms: Iron storage and ferritin expression in diatoms. *Limnol. Oceanogr.* **63**, 1677–1691 (2018).
70. R. H. Lampe *et al.*, Different iron storage strategies among bloom-forming diatoms. *Proc. Natl. Acad. Sci. U.S.A.* **115**, E12275–E12284 (2018).
71. G. Rickard, E. Behrens, CMIP5 earth system models with biogeochemistry: A Ross Sea assessment. *Antarct. Sci.* **28**, 327–346 (2016).
72. K. Petrou, P. Ralph, Photosynthesis and net primary productivity in three Antarctic diatoms: Possible significance for their distribution in the Antarctic marine ecosystem. *Mar. Ecol. Prog. Ser.* **437**, 27–40 (2011).
73. K. Petrou, M. A. Doblin, P. J. Ralph, Heterogeneity in the photoprotective capacity of three Antarctic diatoms during short-term changes in salinity and temperature. *Mar. Biol.* **158**, 1029–1041 (2011).
74. H. Liu *et al.*, Exposure to domoic acid affects larval development of king scallop *Pecten maximus* (Linnaeus, 1758). *Aquat. Toxicol.* **81**, 152–158 (2007).
75. C. A. Scholin *et al.*, Mortality of sea lions along the central California coast linked to a toxic diatom bloom. *Nature* **403**, 80–84 (2000).
76. J. K. Brunson *et al.*, Biosynthesis of the neurotoxin domoic acid in a bloom-forming diatom. *Science* **361**, 1356–1358 (2018).
77. M. W. Silver *et al.*, Toxic diatoms and domoic acid in natural and iron enriched waters of the oceanic Pacific. *Proc. Natl. Acad. Sci. U.S.A.* **107**, 20762–20767 (2010).
78. J. K. Geuer, B. Krock, T. Leefmann, B. P. Koch, Quantification, extractability and stability of dissolved domoic acid within marine dissolved organic matter. *Mar. Chem.* **215**, 103669 (2019).
79. K. R. Arrigo *et al.*, Photophysiology in two major southern ocean phytoplankton taxa: Photosynthesis and growth of *Phaeocystis antarctica* and *Fragilariopsis cylindrus* under different irradiance levels. *Integr. Comp. Biol.* **50**, 950–966 (2010).
80. W. O. Smith *et al.*, Spatial and temporal variations in variable fluorescence in the Ross Sea (Antarctica): Oceanographic correlates and bloom dynamics. *Deep Sea Res. Part I Oceanogr. Res. Pap.* **79**, 141–155 (2013).
81. O. Mangoni *et al.*, *Phaeocystis antarctica* unusual summer bloom in stratified antarctic coastal waters (Terra Nova Bay, Ross Sea). *Mar. Environ. Res.* **151**, 104733 (2019).
82. R. Schmieder, Y. W. Lim, R. Edwards, Identification and removal of ribosomal RNA sequences from metatranscriptomes. *Bioinformatics* **28**, 433–435 (2012).
83. M. Rho, H. Tang, Y. Ye, FragGeneScan: Predicting genes in short and error-prone reads. *Nucleic Acids Res.* **38**, e191 (2010).
84. S. Podell, T. Gaasterland, DarkHorse: A method for genome-wide prediction of horizontal gene transfer. *Genome Biol.* **8**, R16 (2007).
85. R. C. Dugdale, F. P. Wilkerson, The use of ¹⁵N to measure nitrogen uptake in eutrophic oceans; experimental considerations. *Limnol. Oceanogr.* **31**, 673–689 (1986).
86. Loay J. Jabre *et al.*, Data from: Molecular underpinnings and biogeochemical consequences of enhanced diatom growth in a warming Southern Ocean. *Dryad*. <http://datadryad.org/stash/dataset/doi:10.5061/dryad.cjxskn3j>. Deposited 31 July 2020.